# Non-linear interactions of two premixed flames explored by LES with external acoustic forcing

Xingsi Han [1, 2], Aimee S. Morgans [1]

[1] Department of Aeronautics, Imperial College London, South Kensington Campus, London, SW7 2AZ UK

[2] College of Energy and Power Engineering, Nanjing University of Aeronautics and Astronautics, Nanjing 210016, PR China

**Contact:** Xingsi Han (xshan@nuaa.edu.cn), College of Energy and Power Engineering, Nanjing University of Aeronautics and Astronautics, Nanjing 210016, PR China

## Abstract

This paper describes a numerical study of the interactions between two lean premixed flames subjected to external acoustic forcing. This provides insights into the flame-to-flame interactions that may occur during combustion instability in annular combustors. Experimental measurements for comparison are available from the target combustor, developed at Cambridge University (Worth and Dawson, Combustion and Flame, 2012). Large Eddy Simulation (LES) is applied using the open source Computational Fluid Dynamics (CFD) toolbox, OpenFOAM, with the combustion modelled using the PaSR (Partially Stirred Reactor) model with a four-step chemical reaction mechanism for methane/air. Harmonic velocity oscillations are imposed at the inlet; the flame responses are studied based on heat release rate signals in different combustion regions. The effect of the flame separation distance ($S_d$) on both the flame dynamics and unsteady heat release responses is analysed. The results show that the flame-to-flame interactions are non-linear for the flame separations studied. The spatial variation of the unsteady heat release rate demonstrates that flame-wall interactions play an important role, becoming even more important than flame-to-flame interactions for closely spaced flames ($S_d < 2.00D$). These findings imply that for the flame separation distances studied, any flame model used in the low-order annular combustion instability prediction should account for both non-linearity and flame-to-flame interactions.

**Keywords**: Flame interactions, Acoustic forcing, Large eddy simulation, Premixed flame, Combustion instability

## Introduction

Leaner combustion is desired for the new design of gas turbine engines in order to reduce

NO*x* emissions. However, it renders the combustor prone to damaging combustion instabilities (Poinsot and Veynante, 2005; Lieuwen, 2012; Sirignano, 2015). These arise from the coupling of unsteady heat release and acoustics within the combustor. Accurate prediction of combustion instability *a priori* has been a long-standing challenge.

Numerical methods have been developed to model and predict combustion instabilities, and can be classified into two main simulation strategies. The first deals with acoustic waves and unsteady heat release simultaneously via complete 3D compressible CFD calculations (Franzelli et al., 2012). The second method decouples simulations of the acoustic waves and unsteady heat release (Han et al., 2015b; Silva et al., 2013). Due to the very high computational cost of the former, the latter method offers more promise as a practical predictive tool. It typically involves coupling a linear model for the acoustic waves with a flame model to capture the response of unsteady heat release to perturbations (Crocco, 1951; Noiray et al., 2008). The non-linearity of the flame model dictates the features of the limit cycle oscillations resulting from instability, and is generally associated with non-linearity in the underlying flame dynamics (Gicquel et al., 2012; Candel et al., 2014; Emmert et al., 2015).

Large Eddy Simulation (LES) has been used to study the non-linear flame response successfully (Han and Morgans, 2015a; Bauerheim et al., 2015; Krediet et al., 2013) and incorporated into the prediction of combustion instabilities (Han et al., 2015b; Bauerheim et al., 2015). However, most studies concern a single flame excited by a longitudinal acoustic wave, to simulate the plane wave-flame interactions. In many gas turbine combustion chambers, multiple flames are arranged within an annular geometry, and azimuthal modes are also important. Two annular experimental test rigs have recently been independently developed to study annular combustion instabilities; the Cambridge rig (Worth and Dawson, 2013; Dawson and Worth, 2014) and the EM2C Lab rig (Bourgouin et al., 2013; Bourgouin et al., 2015). Both longitudinal and azimuthal mode instabilities are then possible with the latter appearing as standing, rotating (spinning) or slanted modes (Bourgouin et al., 2015). Combustion instabilities in annular combustors have been studied (Dowling and Stow, 2003; Stow and Dowling, 2009; Morgans and Stow, 2007) via low-order network models incorporating a simple flame model. The simplified flame models limit both understanding

and predictive capability - they do not capture the under lying physical mechanisms responsible for the flame response. Instabilities in annular combustors are currently less well understood and methods for accurately incorporating the flame response, particularly if there are flame-to-flame interactions, have not yet been developed.

One significant difference for annular combustor geometries is that flames can interact with neighbouring flames. Experimental measurements have shown that flame-to-flame interactions can strongly affect the flame shapes and the corresponding unsteady heat release (Worth and Dawson, 2012). Recently, a simplified experimental setup consisting of two bluff body stabilised turbulent premixed flames was used to investigate the effect of flame separation distance ($S_d$) on the flame dynamics and unsteady heat release response (Worth and Dawson, 2012). Some of the key physical mechanisms were explored, but experiments were done to measure the global unsteady heat release rate using chemiluminescence methods and one slice of the flow field using cinematographic OH-PLIF measurements. The spatial variation at specific regions and full three-dimensional flame structures are not performed.

This paper intends to complement the experimental study by using high-fidelity LES to study the interactions of two premixed flames subjected to acoustic forcing, based on the experimental rig detailed by Worth and Dawson (2012). The numerical simulations of the flame-to-flame interactions are validated using the experimental data. Full flow field and spatial heat release rate information are then obtained from the LES, allowing more details of the non-linear interactions to be explored. The experimental rig used as a basis for the present study is briefly described in the next section. The numerical large eddy simulations are then described, following with the section focusing on the results and analysis of the LES predictions. Finally, conclusions are drawn in the last section.

## Target experimental test case (Worth and Dawson, 2012)

The target experimental rig consists of two identical bluff-body stabilised turbulent premixed flames placed side by side, as illustrated in Fig. 1(a) and described in detail by Worth and Dawson (2012). For each flame, methane and air are premixed upstream and flow through two concentric ducts, the outer of diameter $D$ = 35 mm and the inner defined by a conical bluff body. The flames are enclosed using a rectangular quartz casing, which is $L$ = 85

mm high and 2$D$ = 70 mm in the spanwise direction. To investigate the effect of flame spacing, three flame separation distances, $S_d$ = 40, 50 and 70 mm are studied, with $S_d$ defined as the distance between the bluff body centres. This corresponds to $S_d$ = 1.14$D$, 1.43$D$ and 2.00$D$. In all cases, the bulk velocity at the combustion chamber inlet is kept constant at $V_b$ = 10.0 m/s (see Fig. 1(b)), giving a Reynolds number of $1.7\times10^4$ based on bluff body diameter. The methane and air are assumed to be fully premixed with an equivalence ratio of $\phi$ = 0.7 for both of the two flames.

For the acoustically forced cases, each plenum was fitted with a pair of loudspeakers mounted diametrically opposite one another. The forcing amplitude ($A$) and frequency ($f$) were varied independently. The heat release rate was measured with global OH* chemiluminescence. For premixed flames, it was also possible to obtain the heat release rate via predicting the Flame Surface Density (FSD) images obtained from OH PLIF measurements at a specific slice of the flow field. The reference velocity in the experiments and simulations was taken at the combustor inlet (the position $P_0$ in Fig. 1(b)).

## Numerical methods for LES

In the present work, large eddy simulations are performed using the CFD toolbox, OpenFOAM, with a modified version of the reactingFOAM solver. The numerical setup for the present LES is similar to that for previous simulations of turbulent partially-premixed combustion (Han et al., 2015b) and fully-premixed combustion (Han et al., 2016). It is based on the low-Mach number LES solver as the flame response is well known to be unaffected by compressibility effects (Lieuwen, 2003).

For turbulence modelling, the one-equation (about subgrid turbulent kinetic energy) transport subgrid scale model is applied (Yoshizawa and Horiuti, 1985). Turbulence and combustion coupling is addressed using the PaSR (Partially Stirred Reactor) combustion model (Fureby, 2012) which has recently drawn attention for premixed flames. An optimized four-step reduced chemical mechanism (Abou-Taouk et al., 2013; Abou-Taouk et al., 2016) for lean methane/air is applied, which captures the laminar premixed flame speed well for equivalence ratios $\phi$ < 1.2. The turbulent mixing time, $\tau_m$, in the PaSR model is modelled based on the subgrid time scale and Kolmogorov time scale, as in previous work (Han et al.,

2015b). Simulation tests were conducted to determine the model constant ($C_m$) for turbulent mixing - a value of 2.0 was chosen for the present LES.

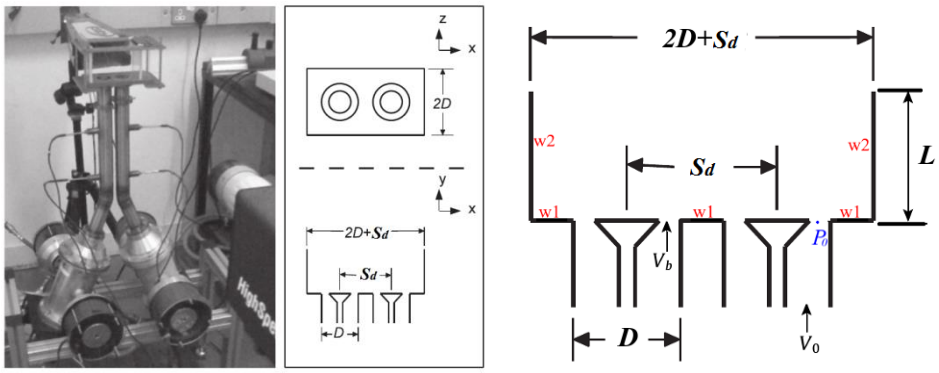


(a) (b)

Figure 1. (a) Schematic of the experimental test case for the two premixed flame combustion chamber (Worth and Dawson, 2012); (b) computational setup for the present LES studies showing a cut ($z$ = 0) of the computational domain, where point $P_0$ is the reference point in the simulations. Solid walls with heat loss are marked *w1* and *w2*.

A schematic $z$-cut of the computational domain is shown in Fig. 1(b). An unstructured mesh is used, with the final mesh, after refinement, containing approximately 2.74, 3.22 and 4.20 million cells for the $S_d$ = 1.14$D$, 1.43$D$ and 2.00$D$ cases respectively. Meshes are clustered near the solid walls with mean $y^+$ around 0.8. To emulate the external acoustic forcing, single frequency harmonic velocities are imposed on the mean flow at the computational inlet with the form (Han et al., 2015b; Krediet et al., 2013):

$$V = V_0\left(1 + A\sin(2\pi ft)\right) + V_{noise} \tag{1}$$

where $V_{noise}$ is added white noise. Significant experimental data is available at a forcing frequency of $f$ = 160 Hz, and so that frequency forms the focus of the present paper, with the forcing amplitude $A$ varying from 0.1 up to 0.4. All the boundaries other than the inlet and outlet are assumed to be solid walls, where no-slip wall conditions are applied. To account for the considerable wall heat loss observed experimentally (see Fig. 1(b)), a lower wall temperature is applied for those walls with heat loss. $T_{w1}$ = 600 K and $T_{w2}$ = 800 K were used, based on previous similar experimental and numerical studies (Han et al., 2015b; Tay-Wo-Chong and Polifke, 2013; Guiberti et al., 2015; Euler et al., 2014) and simulation tests.

To determine the response of the unsteady heat release rate to acoustic forcing, heat release

rate signals are recorded, and the computational domain is divided into different flame regions (see Fig. 2) for integration of the heat release rate. Time average is performed for more than 15000 time steps for unforced cases, and at least 20 forcing cycles have been applied after transients died away in the forced cases.

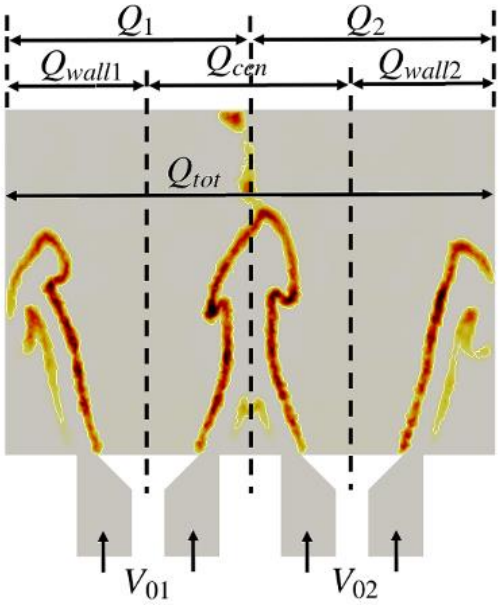


Figure 2. Computational domain for the LES, showing the division into separate flame zones (across the whole span) for the integration of unsteady heat release.

## Results and discussions

### *Unforced reactive flow*

The flame interactions for three separation distances ($S_d$) are firstly examined for the unforced flames. Figure 3 shows the time-averaged volumetric heat release rate from the present LES and the FSD images from the experiments (Worth and Dawson, 2012) at the central cut in the *z*-direction. The present LES predicts the flame shapes, including the interaction region, reasonably well compared to experiments. The "V"-shaped flame corresponding to a single fuel/air inlet is modified in the presence of two flames, due to flame-to-flame interaction in the central region of the combustor and due to interaction with the wall region on the outside. The most important flame-to-flame interaction observation is that the jets and the inner parts of the flame merge along the shear layer from the bluff bodies. Differences can be observed between LES and experiments. The flame brush is less strong in LES to experiments for $S_d = 1.14D$ and $S_d = 1.43D$. The flame anchoring point on the walls changes in LES, while it seems nearly constant in experiment, with varying $S_d$.

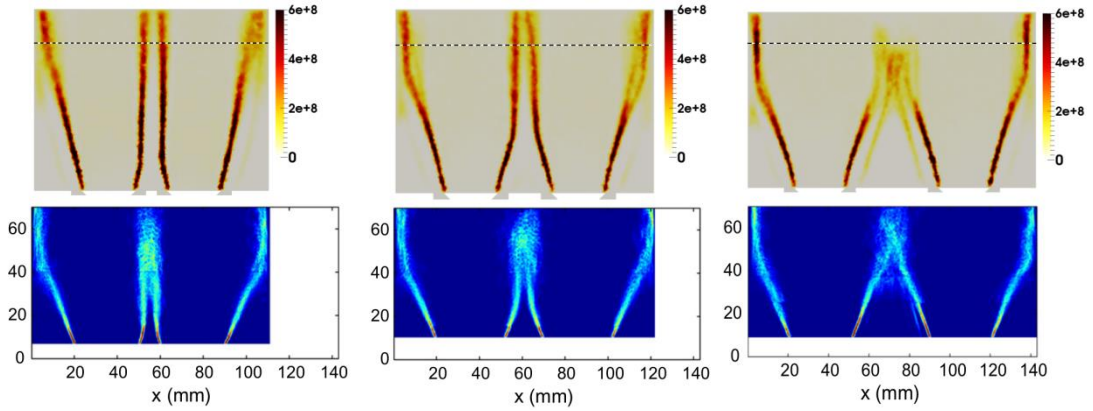


(a) (b) (c)

Figure 3. Time-averaged results of the unforced flames for three separation distances: (a) $S_d$ = 1.14$D$; (b) $S_d$ = 1.43$D$; (c) $S_d$ = 2.00$D$. The volumetric heat release rate in $W/m^3$ from the present LES (top) and the FSD image from experiments (Worth and Dawson, 2012) (bottom), at a $z$-cut of $z$ = 0. The dashed line indicates the upper boundary of the experimental viewing window.

***Forced reactive flow***

When the burner inlet flows have sinusoidal flow oscillations superimposed on them, the flames respond, exhibiting different flame dynamics for different $S_d$. Figure 4 shows the unsteady heat release rate of the flames as predicted by the present LES, for a forcing amplitude of $A$ = 0.3. The three separation distances, at a constant phase angle of around 0 º, are shown. The first observation is that mushroom-shaped flames appear due to vortex-flame interactions, which are similar to those from previous experimental (Balachandran et al., 2005) and numerical (Han and Morgans, 2015a) studies. The inner flame fronts merge into one when the separation distance is small, i.e. $S_d$ = 1.14$D$ and $S_d$ = 1.43$D$, while the two flames can be visually distinguished for the larger separation distance of $S_d$ = 2.00$D$.

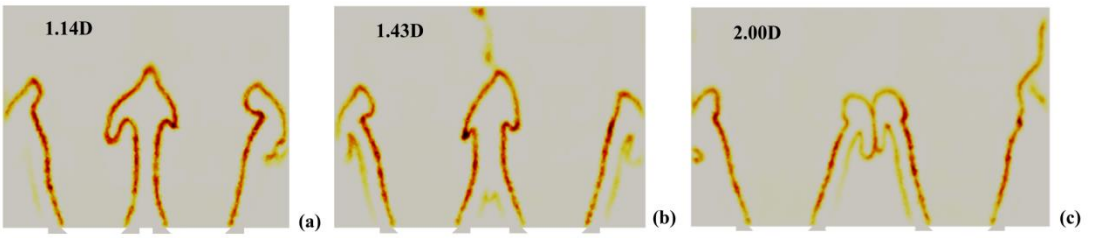


Figure 4. Snapshots of the unsteady heat release rate from the forced flames predicted by the present LES for three separation distances, for forcing with $f$ = 160 Hz and $A$ = 0.3, at phase around 0 º.

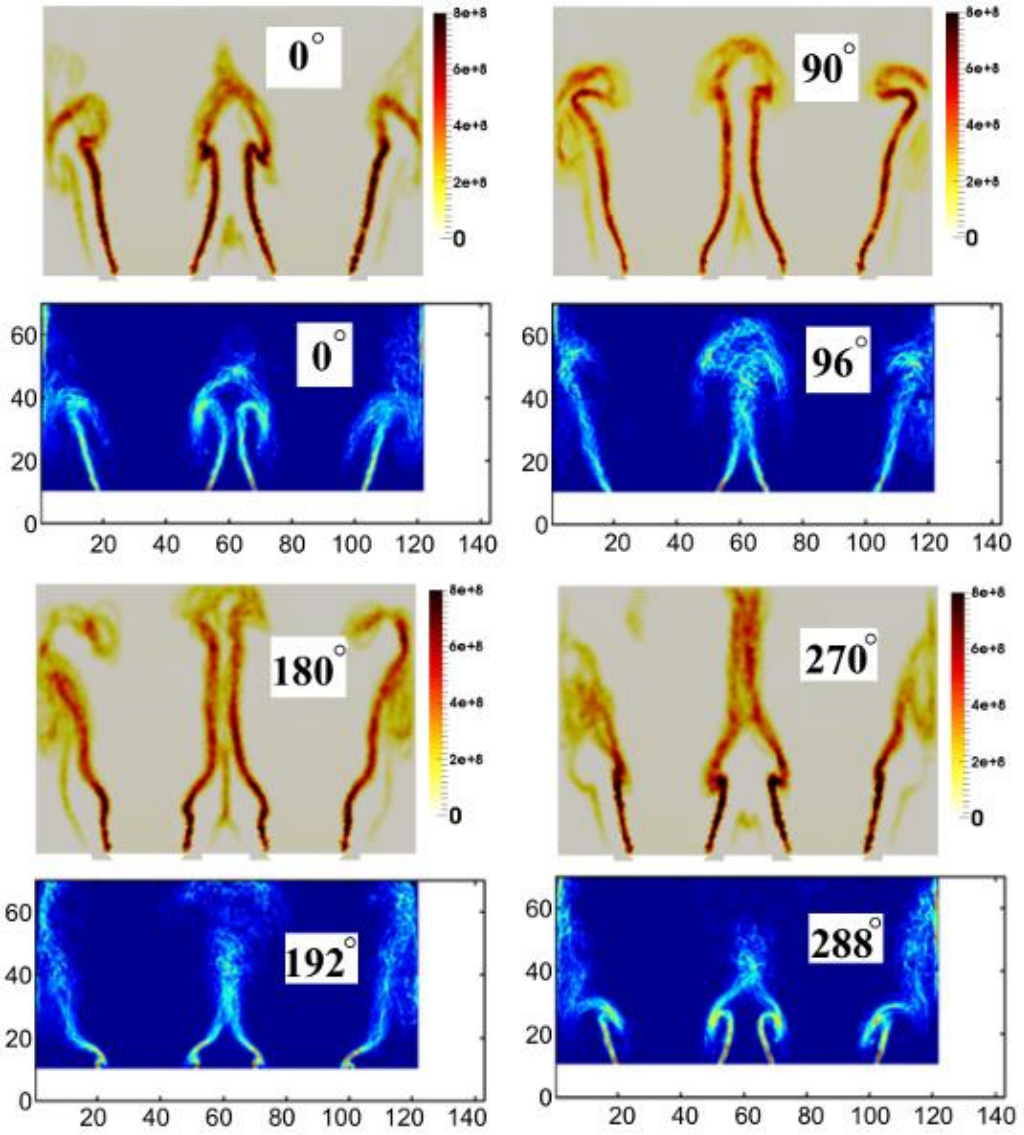


Figure 5. Comparisons of the phase-averaged heat release rate (in $W/m^3$) from the present LES (top) with the FSD image from experiments (Worth and Dawson, 2012) (bottom) at different phase angles. The separation distance is $S_d$ = 1.43$D$, with acoustic forcing at $f$ = 160 Hz and $A$ = 0.32, at a $z$-cut of $z$ = 0.

Figure 5 compares the simulated and experimental sequence of 4 phase-averaged flame images over one forcing cycle with forcing amplitude $A$ = 0.32 for the case $S_d$ = 1.43$D$. It clearly demonstrates the deformation of the two interacting flames at the central region, which roll-up together as a single mushroom. The flame dynamics are otherwise similar to previous observations for a single flame (Han and Morgans, 2015a; Balachandran et al., 2005). The present LES captures the dynamics well compared with experiments.

To investigate whether the effect of the flame interactions can be quantified within the

Flame Describing Function (FDF) framework, two sets of simulation setups are conducted: (I) both of the two fuel/air inlets ($V_{01}$ and $V_{02}$ in Fig. 2) are forced with the form shown in Eq. (1). This is denoted case "N1" in Figs. 6 and 7; (II) only one fuel/air inlet ($V_{01}$ in Fig. 2) is forced with the form shown in Eq. (1); the other inlet $V_{02}$ is not forced, although it still has the imposed constant bulk velocity. This is denoted case "N2". For both cases, the heat release rate attributable to the left and right half regions of the combustor is denoted "$Q1$" and "$Q2$" respectively (see Fig. 2).

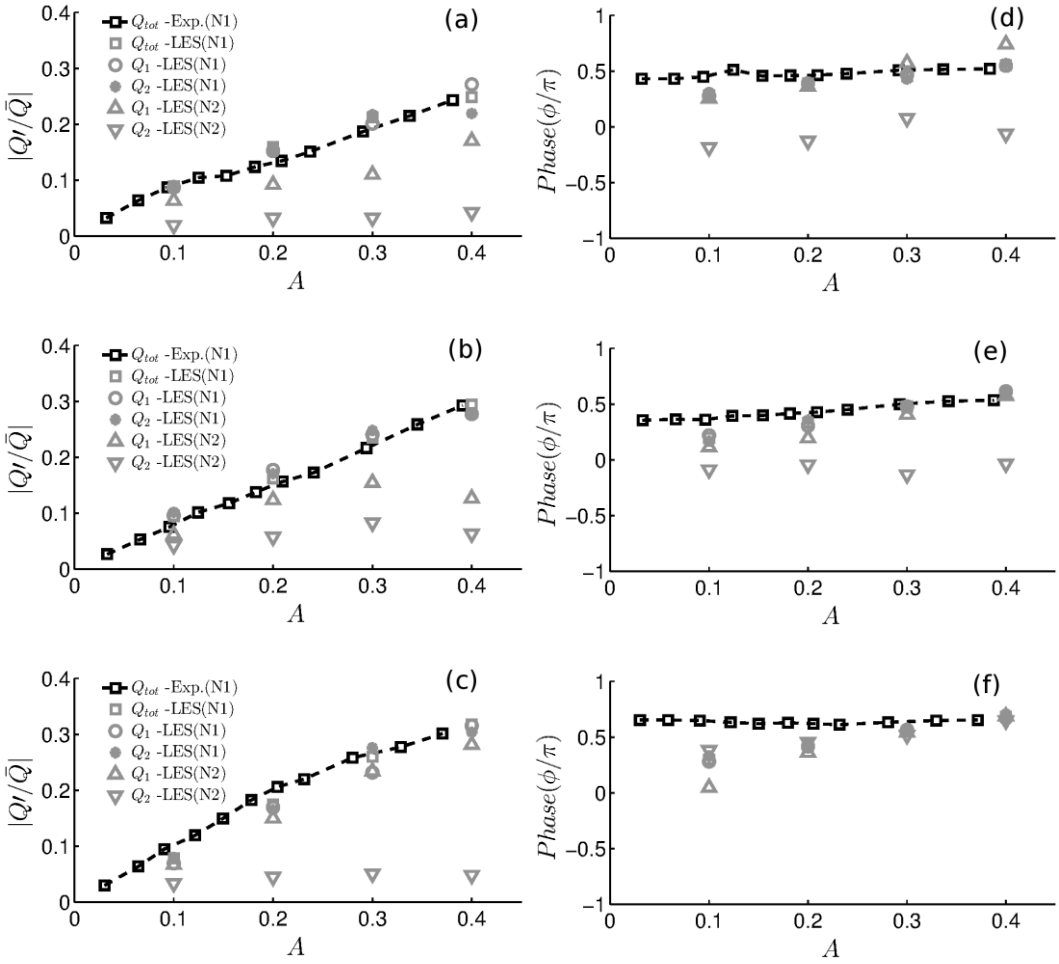


Figure 6. Heat release rate response with velocity fluctuation amplitude $A$: (a) and (d) for $S_d$ = 1.14$D$; (b) and (e) for $S_d$ = 1.43$D$; (c) and (f) for $S_d$ = 2.00$D$, based on integration in different regions of the combustor as in Fig. 2 (left and right regions).

Figure 6 shows the normalised heat release response as a function of the forcing amplitude $A$. The global heat release response predicted by the present LES matches the experimental OH* chemiluminescence measurements reasonably well, for the three separation distances. However, the phase results are less good as the amplitude, which may result from the

turbulence fluctuation at the inlet and white noise cannot accurately represent it. This confirms that the present LES method can predict premixed flame-to-flame interactions with good accuracy. For case N1 with two inlet forcing, the left ($Q_1$) and right ($Q_2$) regions of the flame responses almost match the global response. For case N2 with forcing of only the left inlet, the responses of the left region ($Q_1$) is weakened compared to when both inlets are forced, and the right region still shows some excitation. With increasing separation distance $S_d$, the excitation of the left region generally increases. An exception for $A$ = 0.4 with occurs. The right region shows largest excitation to left acoustic forcing at the intermediate separation distance of $S_d$ = 1.43$D$ as shown in Fig. 6(b) that the heat release response ($Q_2$) has the largest amplitude. This implies that flame-to-flame interaction mechanisms and their dependences on separation distance are complex.

For a linear or weakly nonlinear response regime, for a given forcing amplitude, the two responses of the separate flame regions, $Q_1$ and $Q_2$, would respond to the left and right burner forcing velocities, $V_1$ and $V_2$, such that

$$\begin{bmatrix} Q_1'/\bar{Q} \\ Q_2'/\bar{Q} \end{bmatrix} = \begin{bmatrix} G_{11} & G_{12} \\ G_{21} & G_{22} \end{bmatrix} \begin{bmatrix} V_1'/\bar{V} \\ V_2'/\bar{V} \end{bmatrix} \tag{2}$$

where $G$ denotes Flame Transfer Function (FTF) or Flame Describing Function (FDF), $\bar{Q}$ and $\bar{V}$ are reference values, and $'$ denotes fluctuation. The LES results shown in Fig. 6 can be used to extract the separate matrix elements. If the flame-to-flame interactions are sufficiently linear, then the matrix should be symmetric, such that $G_{11} = G_{22}$ and $G_{12} = G_{21}$, and the single-burner forcing responses should be able to predict the two-burner forcing responses, i.e. $Q_1'/\bar{Q} = G_{11}V_1'/\bar{V} + G_{12}V_2'/\bar{V}$ and $Q_2'/\bar{Q} = G_{21}V_1'/\bar{V} + G_{22}V_2'/\bar{V}$. Note that this superposition of responses to forcing of the separate burners will only hold if the flames interact linearly, and so whether these superposition equations hold provides a key test of the linearity of the flame-to-flame interaction.

Based on the LES predictions in Fig. 6 (using values from the linear regime), for case N2 with $V'_2$ = 0, we can obtain $G_{11}$ and $G_{21}$ (and hence infer $G_{22}$ and $G_{12}$) at $f$ = 160 Hz. The results are summarised in Table 1, where $G_{tot\_sum}$ means summing the separate one-burner responses, $G_{11}$ and $G_{21}$, and $G_{tot\_obs}$ the observed two-burner forcing response from LES of

case N1 for which $V'_1 = V'_2$. Differences can be seen between $G_{tot\_sum}$ and $G_{tot\_obs}$ for all the three separation distances. Both the gain and phase differ significantly for $S_d$ = 1.43$D$, with the main difference being in the gain for $S_d$ = 1.14$D$ and $S_d$ = 2.00$D$. The smallest deviation from superposition holding, and therefore from linearity, is the case with the largest separation distance of $S_d$ = 2.00$D$. Because the two-burner forcing response cannot be accurately recovered by summing the separate one-burner responses, this implies that the flame-to-flame interactions are non-linear across all three separation distances.

Table 1. Comparisons of FTF between summing two one-burner forcing response and the two-burner response.

| | $G_{11}$ | $G_{21}$ | $G_{tot\_sum}=G_{11}+G_{21}$ | $G_{tot\_obs}$ |
|---|---|---|---|---|
| $S_d$=1.14$D$ | $0.47\exp(0.48\pi \mathrm{i})$ | $0.14\exp(-0.075\pi \mathrm{i})$ | $0.47\exp(0.39\pi \mathrm{i})$ | $0.75\exp(0.42\pi \mathrm{i})$ |
| $S_d$=1.43$D$ | $0.52\exp(0.32\pi \mathrm{i})$ | $0.29\exp(-0.076\pi \mathrm{i})$ | $0.66\exp(0.19\pi \mathrm{i})$ | $0.82\exp(0.40\pi \mathrm{i})$ |
| $S_d$=2.00$D$ | $0.72\exp(0.41\pi \mathrm{i})$ | $0.21\exp(0.50\pi \mathrm{i})$ | $0.93\exp(0.43\pi \mathrm{i})$ | $0.83\exp(0.49\pi \mathrm{i})$ |

Another important observation from Figs. 4 and 5 is that the flame-wall interactions seem to have a significant impact on the flame dynamics. In the experiments (Worth and Dawson, 2012), the flames are confined in a rectangular quartz enclosure. This captures the radial wall confinements of flames in real annular combustors, but also introduces false walls "azimuthally". In the study by Worth and Dawson (2012), experimental OH PLIF measurements at a specific slice of $z$ = 0 cut were used to show that the overall trends of the heat release are determined by the changes of flames in the central interacting region, not the wall regions, for all the three separation distances. It should be noted that this observation was limited to a two-dimensional slice, while three-dimensional flame structures can be imagined for the setups presented here. To examine these, the three-dimensional heat release responses in the wall and central interacting regions (see Fig. 2 for the region divide) are extracted from the present LES and shown in Fig. 7. This clearly demonstrates that the flame dynamics in the wall regions dominate the overall dynamics when the flames are close to each other, i.e. $S_d$ = 1.14$D$ and $S_d$ = 1.43$D$, while the flame-to-flame interaction dominates when the flames are further apart, i.e. $S_d$ = 2.00$D$. This is in contrast to the experimental observations, implying

that the heat release response measurement based on two-dimensional OH PLIF has limitations in the present study. Comparing the heat release responses in the central region with two forcing and one forcing (see Fig. 7), it also demonstrates that the flame-flame interactions are highly non-linear when the flames are close to each other, i.e. $S_d$ = 1.14$D$ and $S_d$ = 1.43$D$, and weakly non-linear for $S_d$ = 2.00$D$ with around 12% differences in amplitude. Figure 8 shows the complex three-dimensional flame structures for the three separation distances for a forcing amplitude of $A$ = 0.4. The flames near the walls have complex structures ($S_{wal}$ in Fig. 8), while for the central interaction region ($S_{cen}$ in Fig. 8), the flames increasingly twist with increasing separation distance $S$, resulting in larger heat release rate amplitudes as observed in Figs. 7(a)-(c).

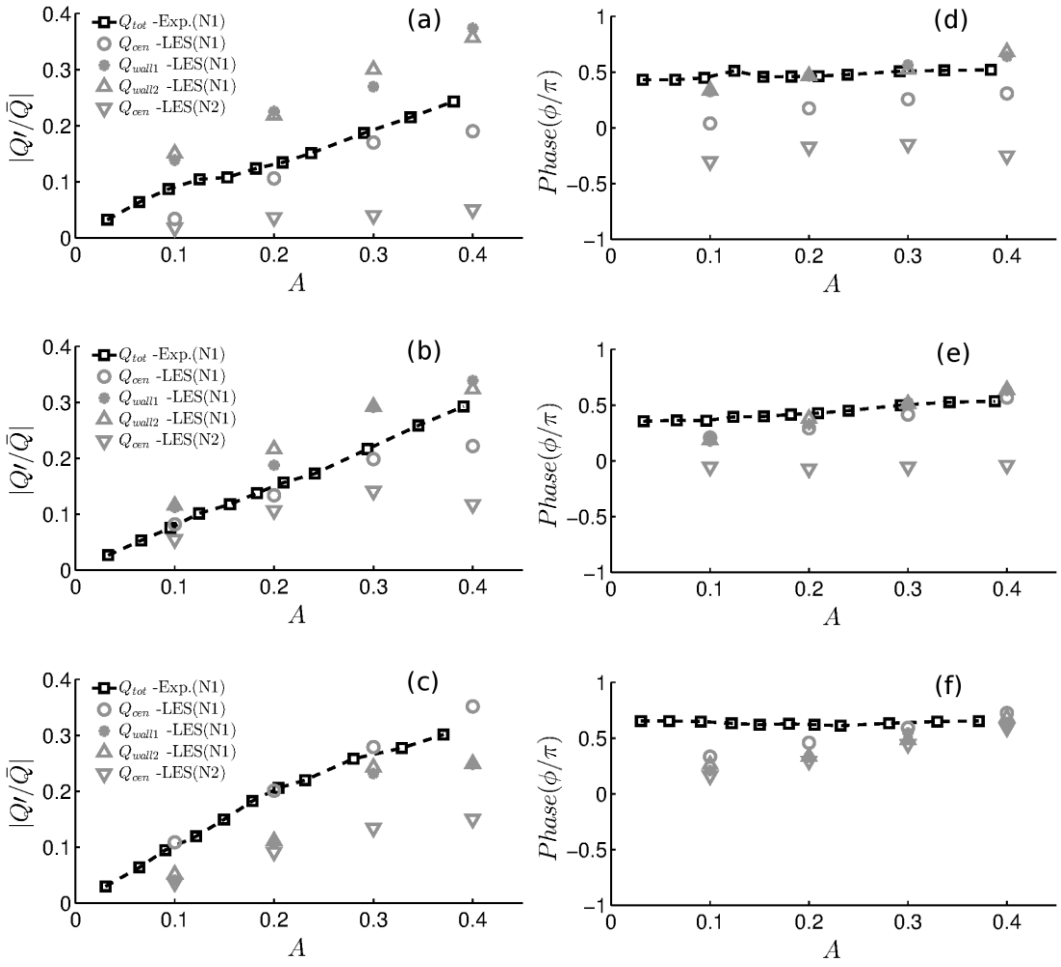


Figure 7. Heat release rate response with velocity fluctuation amplitude $A$: (a) and (d) for $S_d$ = 1.14$D$; (b) and (e) for $S_d$ = 1.43$D$; (c) and (f) for $S_d$ = 2.00$D$, based on integration in different regions of the combustor as in Fig. 2 (central and wall regions).

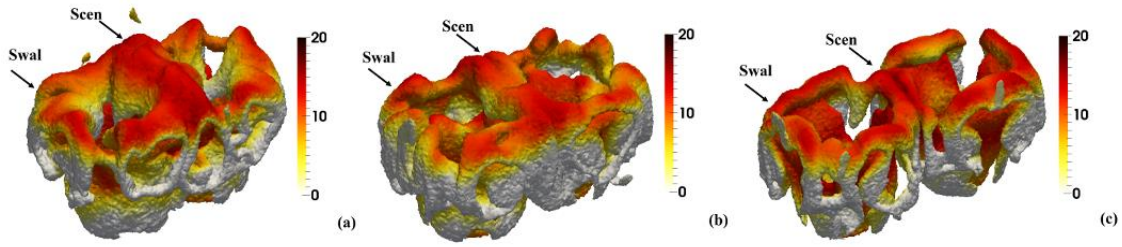


Figure 8. Iso-surfaces of the heat release rate ($Q$ = 1.1×10$^8$$W/m^3$) with three separation distances: (a) $S_d$ = 1.14$D$; (b) $S_d$ = 1.43$D$; (c) $S_d$ = 2.00$D$, at around the phase 90 º, coloured by the axial velocity ($V$). The acoustic forcing is at $f$ = 160 Hz and $A$ = 0.4.

## Conclusions

The present study describes an analysis based on large eddy simulations of two interacting premixed flames, excited by external acoustic forcing for three flame separation distances. Numerical predictions are compared with available experimental measurements, with reasonably good agreement observed for both the unforced and forced flames, although differences between them can be observed. The two flames interact in a central region, merging into one another when sufficiently close, i.e. $S_d$ < 2.00$D$. They generally behave as two isolated flames when further apart, i.e. $S_d$ = 2.00$D$. When excited by acoustic forcing, a single mushroom-shaped flame appears and evolves in the central region for the two smaller flame separations, with two evolving mushroom-shaped flames visually observed for the larger flame separation. A superposition analysis based on the LES results demonstrates that the flame-to-flame interactions are all non-linear for the cases presented here. Flame modelling used in low-order modelling of annular combustors therefore may need to account for both non-linearity and flame-to-flame interactions if the flames are spaced sufficiently closely. Findings from the present study also reveal flame-wall interactions to be very important, even more so than flame-to-flame interactions for closely spaced flames. Finally, the LES findings also suggest that, for complex and interacting three-dimensional flame structures encountered in annular combustors, high-fidelity LES may prove a useful tool for obtaining insights into such flames in the future.

## Acknowledgements

This work is financially supported by the European Research Council via the ERC Starting

Grant, ACOULOMODE (2013-18), the National Natural Science Foundation of China (grand No: 51606095), the Jiangsu Provincial Natural Science Foundation of China (grand No: BK20160794) and the Fundamental Research Funds for the Central Universities. Computational time on the UK National Supercomputing Service ARCHER and the CX1 HPC cluster at Imperial College London is gratefully acknowledged.

## References

Abou-Taouk, A., Sadasivuni, S., Lorstad, D., and Eriksson, L.-E. 2013. Evaluation of global mechanisms for LES analysis of SGT-100 DLE combustion system. Presented at the ASME Turbo Expo, June 3-7, San Antonio, Texas, USA. Paper No. GT2013-95454.

Abou-Taouk, A., Farcy, B., Domingo, P., Vervisch, L., Sadasivuni, S., Eriksson, L.-E. 2016. Optimized Reduced Chemistry and Molecular Transport for Large Eddy Simulation of Partially Premixed Combustion in a Gas Turbine. *Combust. Sci. Tech.*, 188, 21 – 39.

Balachandran, R., Ayoola, B.O., Kaminski, C.F., Dowling, A.P., and Mastorakos E. 2005. Experimental investigation of the nonlinear response of turbulent premixed flames to imposed inlet velocity oscillations. *Combust. Flame*, 143, 37 – 55.

Bauerheim, M., Staffelbach, G., Worth, N.A., Dawson, J.R., Gicquel, L.Y.M., and Poinsot, T. 2015. Sensitivity of LES-based harmonic flame response model for turbulent swirled flames and impact on the stability of azimuthal modes. *Proc. Combust. Inst.*, 35, 3355 - 3363.

Bourgouin, J.F., Durox, D., Schuller, T., Beaunier, J., and Candel, S. 2013. Ignition dynamics of an annular combustor equipped with multiple swirling injectors. *Combust. Flame*, 160, 1398 – 1413.

Bourgouin, J.F., Durox, D., Moeck, J.P., Schuller, T., and Candel, S. 2015. A new pattern of instability observed in an annular combustor: The slanted mode. *Proc. Combust. Inst.*, 35, 3237 – 3244.

Candel, S., Durox, D., Schuller, T., Bourgouin, J.F., and Moeck, J.P. 2014. Dynamics of Swirling Flames. *Annu. Rev. Fluid Mech.*, 46, 147 - 173.

Crocco, L. 1951. Aspects of combustion stability in liquid propellant rocket motors Part I: fundamentals. Low frequency instability with monopropellants. *J. Am. Rocket Soc.*, 21, 163 - 178.

Dawson, J.R., Worth, N.A. 2014. Flame dynamics and unsteady heat release rate of self-excited azimuthal modes in an annular combustor. *Combust. Flame*, 161, 2565 – 2578.

Dowling, A.P., and Stow, S.R. 2003. Acoustic analysis of gas turbine combustors. *J. Propul. Power*, 19, 751 – 763.

Emmert, T., Bomberg, S., and Polifke, W. 2015. Intrinsic thermoacoustic instability of premixed flames. *Combust. Flame*, 162, 75 - 85.

Euler, M., Zhou, R., Hochgreb, S., Dreizler, A. 2014. Temperature measurements of the bluff body surface of a Swirl Burner using phosphor thermometry. *Combust. Flame*, 161, 2842 – 2848.

Franzelli, B., Riber, E., Gicquel, L.Y.M., and Poinsot, T. 2012. Large Eddy Simulation of combustion instabilities in a lean partially premixed swirled flame. *Combust. Flame*, 159, 621 - 637.

Fureby, C. 2012. A Comparative Study of Flamelet and Finite Rate Chemistry LES for a Swirl Stabilized Flame. *J. Eng. Gas Turb. Power*, 134, 041503.

Gicquel, L.Y.M., Staffelbach, G., and Poinsot, T. 2012. Large eddy simulations of gaseous flames in gas turbine combustion chambers. *Prog. Energy Combust. Sci.*, 38, 782 - 817.

Guiberti, T.F., Durox, D., Scouflaire, P., Schuller, T. 2015. Impact of heat loss and hydrogen enrichment on the shape of confined swirling flames. *Proc. Combust. Inst.*, 35, 1385 – 1392.

Han, X., Morgans, A.S. 2015a. Simulation of the flame describing function of a turbulent premixed flame using an open-source LES solver. *Combust. Flame*, 162, 1778 - 1792.

Han, X., Li, J., and Morgans, A.S. 2015b. Prediction of combustion instability limit cycle oscillations by combining flame describing function simulations with a thermoacoustic network model. *Combust. Flame*, 162, 3632 - 3647.

Han, X., Yang, J., and Mao J. 2016. LES investigation of two frequency effects on acoustically forced premixed flame. *Fuel*, 185, 449 – 459.

Krediet, H.J., Beck, C.H., Krebs, W., and Kok, J.B.W. 2013. Saturation mechanism of the heat release response of a premixed swirl flame using LES. *Proc. Combust. Inst.*, 34, 1223 - 1230.

Lieuwen, T. 2003. Modeling premixed combustion-acoustic wave interactions: A review. *J. Propul. Power*, 19, 765 – 781.

Lieuwen, T.C. 2012. *Unsteady combustor physics*, Cambridge University Press, New York.

Morgans, A.S., Stow, S.R. 2007. Model-based control of combustion instabilities in annular combustors. *Combust. Flame*, 150, 380 – 399.

Noiray, N., Durox, D., Schuller, T., and Candel, S. 2008. A unified framework for nonlinear combustion instability analysis based on the flame describing function. *J. Fluid Mech.*, 615, 139 - 167.

Poinsot, T., Veynante, D. 2005. *Theoretical and Numerical Combustion*, 2nd Edition, R.T. Edwards, PA, USA.

Silva, C.F., Nicoud, F., Schuller, T., Durox, D., and Candel, S. 2013. Combining a Helmholtz solver with the flame describing function to assess combustion instability in a premixed swirled combustor. *Combust. Flame*, 160, 1743 - 1754.

Sirignano, W.A. 2015. Driving Mechanisms for Combustion Instability. *Combust. Sci. Tech.*, 187, 162 – 205.

Stow, S.R., and Dowling, A.P. 2009. A Time-Domain Network Model for Nonlinear Thermoacoustic Oscillations. *J. Eng. Gas Turb. Power*, 131, 031502.

Tay-Wo-Chong, L., and Polifke, W. 2013. Large Eddy Simulation-Based Study of the Influence of Thermal Boundary Condition and Combustor Confinement on Premix Flame Transfer Functions. *J. Eng. Gas Turb. Power*, 135, 021502.

Worth, N.A., and Dawson, J.R. 2012. Cinematographic OH-PLIF measurements of two interacting turbulent premixed flames with and without acoustic forcing. *Combust. Flame*, 159, 1109 – 1126.

Worth, N.A., and Dawson, J.R. 2013. Self-excited circumferential instabilities in a model annular gas turbine combustor: Global flame dynamics. *Proc. Combust. Inst.*, 34, 3127 – 3134.

Yoshizawa, A., and Horiuti, K. 1985. A Statistically-Derived Subgrid-Scale Kinetic Energy Model for the Large-Eddy Simulation of Turbulent Flows. *J. Phys. Soc. Jpn.*, 54, 2834 – 2839.